Phys Chem Minerals (2003) 30: 345–352
DOI 10.1007/s00269-003-0323-5

ORIGINAL PAPER

K. Kihara · N. Matsui

Molecular dynamics study and normal mode analysis of diffuse scattering in quartz

Received: 24 October 2002 / Accepted: 9 April 2003

Abstract X-ray scattering intensities in quartz were investigated in molecular dynamics (MD) simulation at different temperatures with the aid of normal mode analyses. The MD-simulated structure produced diffuse streaks most remarkably along a hexagon joining symmetry-equivalent points of index 400 in the hk0 plane, extending in ± **c***. In addition, most Bragg spots were found to be associated by radial diffuse scattering in the six **a*** directions. The normal mode analysis and calculations of first-order scattering intensities showed that the lowest-lying branch in Γ-M is of transversal acoustic characters, and is responsible for the diffuse scattering radiating from Bragg reflections in the **a***-directions. The transversal acoustic characters of atomic displacements in these modes provide the scattering in phase at points on the fourth hexagon. Phonon dispersion relations of the MD crystal were examined in view of symmetry-adapted atomic displacement patterns, and a possibility was suggested for two curves in Γ-M, optic soft branch and transversal acoustic branch polarized in the *z* axis (the second-lowest branch), to exchange the eigenvectors in the middle range of **q** (0.2–0.3).

Keywords Quartz · Diffuse scattering · Molecular dynamics simulation · Normal mode analysis

Introduction

The structure of quartz (SiO_2) has space group $P3_221$ or $P3_121$ for phase α and $P6_222$ or $P6_422$ for β. In some ranges of temperature around the α–β transition point, characteristic non-radial diffuse streaks along a line joining the reciprocal lattice points 400 and 040 and its symmetry-equivalent lines were observed in the hk0 plane of an X-ray oscillation photograph (Arnold 1965). This diffuse scattering along the "fourth hexagon" (FH) is also observed in electron diffraction patterns of quartz and berlinite, a quartz form of $AlPO_4$ (Tendeloo et al. 1976). The electron diffraction study further showed that the diffuse scattering in the FH is planar, extending parallel to the *c* axis, rather than rods. The diffuse scattering (abbreviated as DS hereafter) is present in both the α and β phases, but is especially intense around the transition point (Arnold 1965). This DS was first considered by Arnold to be of elastic origin. However, Bauer et al. (1971) were not able to observe elastic scattering in their neutron study, but observed that phonon frequencies are highly anisotropic and especially low for the Γ-M directions, which they considered to be the cause of the enhanced X-ray scattering in the diffuse streaks. Tendeloo et al. (1976) found that the DS in the α phases arises within each of the microscopic domains appearing near the transition point. These electron microscopic observations led Tendeloo et al. to believe that DS is dynamic in nature rather than static, being concordant with Bauer et al. (1971) conclusion based on the inelastic origin.

A microscopic lattice dynamical model of the DS at the M-point mode was already given by Boysen et al. (1980) in the inelastic neutron scattering study. Vallade et al. (1992) showed the pattern of the FH calculated on rigid tetrahedral SiO_4 (RTM) modes in their interpretation of inelastic neutron scattering in β-quartz. These authors also calculated inelastic neutron scattering structure factors for various RTM modes, and showed that the temperature-dependent Σ_2 mode make a major contribution to the DS.

The molecular dynamics (MD) approach has been adopted by many authors as a powerful tool for studying the structural changes and physical properties in quartz (Tsuneyuki et al. 1990; Miyake et al. 1998; Kihara 2001; Müser and Binder 2001 etc.). The present study was motivated to draw detailed atomic pictures causing DS in quartz by applying MD simulations. During the study, we found an interesting relation for atomic polarization vectors between the soft optic mode

K. Kihara · N. Matsui (✉)
Department of Earth Sciences, Kanazawa University,
Kanazawa 920-1192, Japan
e-mail: kuniaki@kenroku.kanazawa-u.ac.jp

and transversal acoustic mode polarized in **c**, although these modes were found to have less effect on DS the two branches in Γ-M could exchange their polarization vectors halfway between the Γ and M points.

Among the many approaches to studying the incommensurate (INC) phase known to occur between the α and β phases, neutron inelastic scattering measurement may provide straightforward evidence. According to such studies, two branches along Γ-M, i.e. the optic soft branch and the lowest-frequency acoustic branch polarized in (001), couple strongly with each other, causing an anticrossing at small **q** ($\ll$ 0.1a*) (see, e.g. Berge et al. 1986). Our present results for the MD crystal show another possibility of anticrossing between the soft mode (SM) and another transversal mode polarized perpendicular to (001), but at a larger **q** between 0.2 and 0.3a* in a wide temperature range through the α and β phases.

A constant-temperature and constant-pressure MD simulation (NTP MD) was carried out, and scattering intensity distribution was calculated for the atomic trajectory data. In this paper, we report first the DS of the MD crystal, and then the results of eigenvector analysis of low-frequency modes in relation with the DS, based on the atomic trajectories in the MD, and finally the dispersion relations with eigenvector exchange.

Calculations

Molecular dynamics simulation

In this study, we conducted the MD calculations using the same energy parameters as in our previous study (Kihara 2001), but with a different MD box of (10 × 10 × 10) hexagonal cells, where 9000 atoms are involved. The time-averaged structural values such as atomic fractional coordinates, atomic mean square displacements etc. for the NPT ensemble simulations were found to be essentially equal to those of the previous results with different system sizes. In the NPT system, the structure certainly transforms between the trigonal (we chose $P3_221$) and the hexagonal ($P6_222$) structures, and the temperature evolution of c/a shows an anomaly at about 800 K, although the values are approximately 0.02 smaller than those for the experiment at each temperature (Fig. 1). These and other data such as the temperature dependences in cell dimensions, atomic fractional coordinates, atomic transfer rates over α_1 and α_2 sites, SM frequency etc. indicate that the α–β transition takes place above 800 K in this system. Among these data, the fractional coordinates of atoms, averaged over 1000 hexagonal unit cells and 40 960 steps (40.96 ps), were found to give the clearest idea about the transition point: the structure is still in the α phase at 800 K, but already in the β phase at 830 K.

In the present study, we first calculated X-ray scattering intensities from the MD crystal with 9000 atoms, and then low-frequency modes were analyzed with respect to the contribution to the DS.

Scattering intensities

X-ray scattering intensities in electron units from the MD crystal were calculated for the atomic trajectories using

$$\mathrm{I}(\mathbf{Q}) = \langle \mathrm{Y}*(\mathbf{Q},\ t)\mathrm{Y}(\mathbf{Q},\ t)\rangle \qquad (1)$$

with

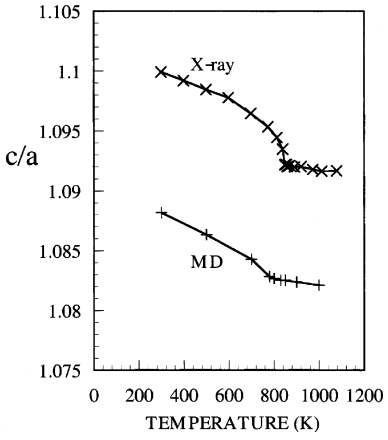

Fig. 1 Temperature dependence of c/a ratio in a molecular dynamics quartz structure in comparison with that in an X-ray study (Kihara 1990). *Lines* connect data points

$$\mathrm{Y}(\mathbf{Q},t) = \sum_k f_k(\mathbf{Q}) \exp i[\mathbf{Q}\cdot\mathbf{r}(k,t)]\ ,$$

where $\langle .....\rangle$ is the time average of the quantity embodied, $f_k(\mathbf{Q})$ and $\mathbf{r}(k,t)$ are the scattering factor and position vector at time t of atom k (from 1 to 9000), respectively, and **Q** the scattering vectors. The time average was taken by accumulating the intensities calculated at the 4096 points stored at every tenth step of the 40 960 steps. The calculations were undertaken for **Q** at the "reciprocal lattice" nodes of the MD cell with edges of the 10 × 10 × 10 hexagonal unit cells. In this study, intensities (in electron units) are given per atom and per time step.

First-order diffuse scattering

The DS contribution to the intensities calculated with Eq. (1) is analyzed for low-frequency phonon modes. The intensity at scattering vector **Q** is expanded in a power series in rewriting Eq. (1), where the first- and higher-order terms represent DS (Willis and Pryor 1970). The higher-order terms were neglected as usual, and DS was represented by the first-order term, I_1, which is proportional to the square of the first-order dynamical structure factor $F_1(\mathbf{Q}, j\mathbf{q})$,

$$\mathrm{I}_1(j\mathbf{q}) = \frac{1}{N}\frac{E_j(\mathbf{q})}{\omega_j^2(\mathbf{q})}|F_1(\mathbf{Q},j\mathbf{q})|^2\ , \qquad (2)$$

where $E_j(\mathbf{q})$ is the energy of phonon $j\mathbf{q}$, $\omega_j(\mathbf{q})$ frequency and N the number of primitive unit cells in the system. The dynamical structure factor at **Q** is calculated using a relation:

$$F_1(\mathbf{Q},j\mathbf{q}) = \sum_k m_k^{-1/2} f_k(\mathbf{Q}) \exp[-W_k(\mathbf{Q})] \\ [\mathbf{Q}\cdot\mathbf{e}(k|j\mathbf{q})] \exp[2\pi i\mathbf{H}\cdot\mathbf{r}(k)]\ , \qquad (3)$$

where $\mathbf{e}(k|j\mathbf{q})$ is the polarization vector of atom k in mode $j\mathbf{q}$, m_k and W_k are the mass and Debye–Waller factor of atom k, respectively, and the summation is taken for the primitive cell. In Eq. (3), scattering vector **Q** is expressed using a reciprocal lattice vector **H** and a wave vector **q**, $\mathbf{Q} = 2\pi(\mathbf{H} + \mathbf{q})$. The polarization vectors were obtained from the atomic trajectories in the procedure explained below. Firstly, an α-th Cartesian component of a time-dependent collective quantity, $U_\alpha(k,\ \mathbf{q},\ t)$, is defined as a mass-adjusted Fourier component of the displacement of atom k in unit cell ℓ from the mean positions, $u_\alpha\ (k,\ \ell,\ t)$, as

$$U_\alpha(k,\mathbf{q},t) = \left(\frac{m_k}{N}\right)^{1/2}\sum_\ell u_\alpha(k,\ell,t)\exp\{2\pi i[\mathbf{q}\cdot\mathbf{R}(k,\ell)]\}\ , \qquad (4)$$

where $\mathbf{R}(k, \ell)$ is the time-averaged position vector of the k-th atom in the ℓ-th unit cell (see, e.g. Dove 1987). $U_\alpha(k, \mathbf{q}, t)$ s with $\alpha = 1, 2$ and 3 are rearranged in a column vector $U_j(\mathbf{q}, t)$ by placing in the order of k:j runs from 1 to $3n$, the number of phonon branches. The polarization vectors and the amplitudes of the $3n$ modes were estimated in solving a characteristic equation:

$$\mathbf{Me} = \delta^2 \mathbf{e} \ , \tag{5}$$

where $\mathbf{M}$ is a $(3n \times 3n)$ matrix with elements of $\langle U_i(\mathbf{q}, t) U_j(\mathbf{q}, t)^* \rangle$, and the time average is taken. The square root of the eigenvalues, δ, may give the amplitudes of excitation. In the present case, $n = 9$, k and ℓ reach 9 and 1000, respectively, and the average was taken for 4096 steps stored at every tenth step of 40 960 MD steps (40.96 ps).

Results

Diffuse scattering of MD crystal

In this paper, the reciprocal lattice vector $\mathbf{H}$ and wave vector $\mathbf{q}$ are expressed on the basis of the hexagonal reciprocal lattice coordinates, $\mathbf{a}^*$, $\mathbf{b}^*$ and $\mathbf{c}^*$, i.e. $\mathbf{H}$ or $\mathbf{q} = \xi\mathbf{a}^* + \eta\mathbf{b}^* + \zeta\mathbf{c}^*$: for the latter, the absolute values of indices ξ, η and ζ are smaller than or equal to 0.5. Points in the Brillouin zone are expressed in the conventional way: Greek letter Γ represents the zone centre 000, and M, K and A the zone boundary points on $\mathbf{a}^*$, $\xi\xi 0$ and $\mathbf{c}^*$, respectively. Points on the Γ-M, Γ-K and Γ-A lines, except at both ends, are expressed with Σ, Λ and Δ, respectively.

Figure 2a exhibits the scattering intensities calculated with Eq. (1) at grid points separated from each other by 0.2 in both $\mathbf{a}^*$ and $\mathbf{b}^*$ in the section at $\zeta = 0$ at different temperatures, and Fig. 2b at $\zeta = 0.4$, 1.0, 2.0 and 3.0 at 1000 K. The intensity distribution appears to nearly satisfy the expected trigonal or hexagonal Laue symmetry at each temperature. At high temperatures, characteristic non-radial DS patterns are observed. Among these, the most remarkable is the FH in the $\xi\eta 0$ plane, which is already recognizable above the background at 500 K, and becomes stronger with increasing temperature in the α phase. The DS along the FH extends over non-zero fractional values of ζ to form a hexagonal prism rather than a ring (Fig. 2b): this is already observed in the electron diffraction study by Tendeloo et al. (1976). Non-radial diffuse streaks also appear in higher reciprocal lattice planes, but in inner hexagons parallel with the FH. Among these, the second hexagon in the $\xi\eta 3$ plane is prominent (Fig. 2b), but these DS have not been explicitly noted in previous studies, because the intensities are probably not as strong as for the FH in the $\xi\eta 0$ plane.

Figure 3 shows the temperature evolution of the intensities at $\overline{1.5}$ 4 0, together with the X-ray observation in a quartz crystal (Arnold 1965). The diffuse intensities increase with temperature up to the transition temperature, and then begin to fall in both the X-ray measurement and the MD simulation. The intensities for the MD case show an increasing trend above about 900 K, whereas no X-ray measurement was reported above that temperature.

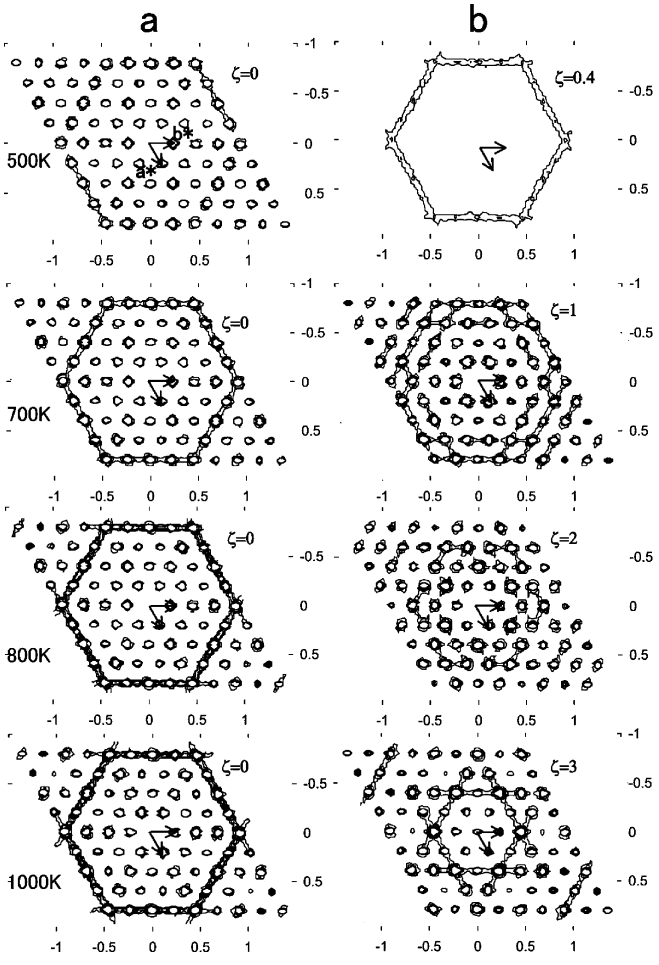

Fig. 2a,b Total intensity distribution from a quartz crystal in molecular dynamics simulation. Intensities (in electron units) per atom and per time step are shown in *sections perpendicular to c**. *Contours* are from 20 to 240 with increments of 20, and omitted if higher than 240. **a** $\xi\eta 0$ planes at different temperatures, where reflection 000 is omitted. **b** Four different sections with heights $\zeta = 0.4$, 1, 2 and 3 at 1000 K. Note that no reflection except 003 appears along 00ℓ: the expected systematic absence is certainly observed. *Scales* indicated in vertical and horizontal directions are reciprocal lattice coordinates in Å^{-1}

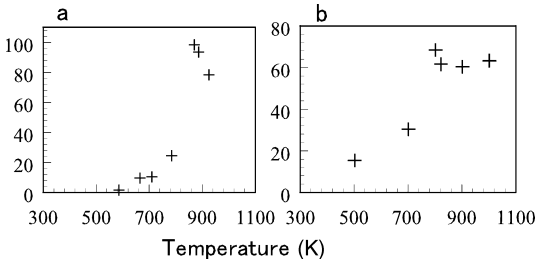

Fig. 3a,b Temperature evolution of diffuse scattering intensity at $\overline{1.5}$ 4 0 in a quartz structure simulated in molecular dynamics calculations in comparison with that in an X-ray study. **a** X-ray values are read from a figure given by Arnold (1965) and shown in an arbitrary scale. Values in **b** (Molecular dynamics) including background intensities, and the same contour levels as for Fig. 2 are applied

In addition to the non-radial DS, in our intensity maps (Fig. 2), a number of Bragg spots appear to be associated by radiating DS along the six or other **a***-equivalent direction. The appearance of this type of DS is also strongly temperature-dependent, becoming more remarkable with increasing temperature. Figure 4 shows such DS around Bragg spots 1 $\overline{2}$ 2 (left) and 203 (right) at 300, 820 and 1000 K (Fig. 4a–c, respectively) for grid separations reduced to 0.1 in both **a*** and **b***. This type of temperature-dependent DS as mentioned later, is related to INC satellite reflections observed in detailed neutron elastic scattering observations (Dolino et al. 1984) or other high-resolution diffraction measurements using, for example, synchrotron radiation (Zarka et al. 1988; Ohsumi et al. 2002) or fine-beam Laue technique (Gouhara et al. 1983).

First-order scattering intensities from low-frequency modes

The first-order scattering intensities calculated for the three acoustic and one optic soft branches in Γ-M, Γ-K and Γ-A are illustrated in Fig. 5 for the Bragg spots, 4 $\overline{3}$ 0, 4 $\overline{2}$ 0, 1 $\overline{2}$ 2 and 203 at 1000 K. $E_j(\mathbf{q})/\omega_j^2(\mathbf{q})$ in Eq. (2) was represented by $\delta(j\mathbf{q})^2$, the eigenvalues of Eq. (5). We found that the lowest-frequency branches in Γ-M and Γ-A predominantly contribute to the DS around 4 $\overline{3}$ 0 and 4 $\overline{2}$ 0, both in the FH (Fig. 5). However, this is not necessarily applicable to all the cases; for example, the DS streaks around reflection 203 and 1 $\overline{2}$ 2 are largely contributed by both the lowest and the third-lowest branches (Fig. 5d). Among these different situations for different reflections, the most noticeable is that the DS streaks in the FH come mostly from the lowest branch (Fig. 5a,b). On the other hand, the Γ-K branch shows less significant diffuse intensities for all the reflections examined.

Dispersion relations of low-frequency modes

The frequencies of modes, except for the acoustic modes at Γ, were approximated by the values of $\{k_B\ T/\delta^2(j\mathbf{q})\}^{1/2}$, which may represent quasiharmonic frequencies (Dove 1993). The dispersion relations of the four low-frequency branches were constructed in examining the continuity of the eigenvectors at neighbouring pairs of **q** separated by 0.1 on Γ-M, Γ-K and Γ-A, consulting with the given symmetries and the results of lattice dynamical calculations. Group-theoretical analysis of normal modes based on Worlton and Warren (1972) was very helpful in examining the eigenvectors in the present study.

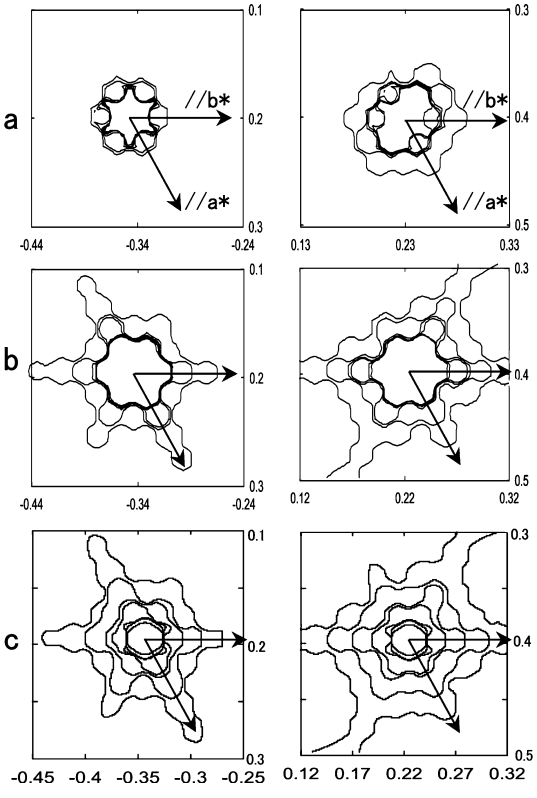

Fig. 4a–c Close views of total intensity distribution and its temperature dependence around reflections 1 $\overline{2}$ 2 (*left*) and 203 (*right*) at **a** 300, **b** 820 and **c** 1000 K in a molecular dynamics simulation of quartz. *Scales* indicated in *vertical and horizontal directions* are reciprocal lattice coordinates in Å^{-1}. *Contours*, levels as for Fig. 2, are from 20 to 120 with increment 20, and omitted if higher than 120

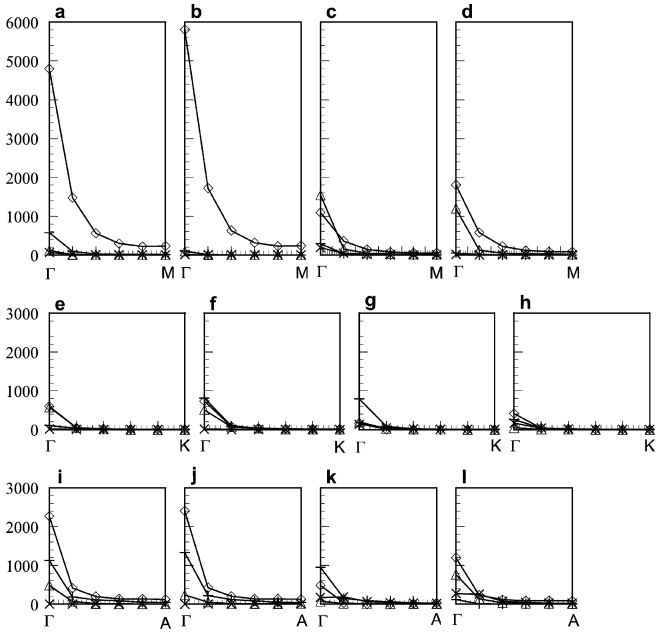

Fig. 5a–l Calculated first-order scattering intensities (in arbitrary units) from three acoustic and one optic branches in three directions for 4 $\overline{3}$ 0, 4 $\overline{2}$ 0, 1 $\overline{2}$ 2 and 203 reflections *from the left* at 1000 K. **a** to **d** For Γ-M, **e** to **h** for Γ-K and **i** to **l** for Γ-A. Diamonds lowest acoustic branch; plus signs second-lowest acoustic branch; triangles third-lowest acoustic branch; crosses optic soft branch

The dispersion curves determined in this way are shown in Fig. 6 for the three acoustic and one optic branches in Γ-M at 500, 700, 800 and 1000 K: in the case for 1000 K, two other directions, Γ-K and Γ-A, are also shown. The Γ-point frequencies of the acoustic modes are set to zero in drawing the curves (Appendix 1). The dispersion relations in the low-frequency branches in the three directions are described below, where the three acoustic branches are distinguished by showing the major components at small **q** in parentheses after letters TA (transversal acoustic) or LA (longitudinal acoustic): the two TA branches may sometimes be indicated as TA_1 for the lower branch or TA_2 for higher branch.

Γ-*M branches*

The four low-frequency dispersion curves in the β phase at 1000 K are in especially good agreement with those of the neutron measurements at 1250 K (Dolino et al. 1992) as far as their appearance is concerned. The optic branch in the α phase, which has the atomic displacement pattern at Γ complying with the A_1 representation (rep), shows remarkable temperature dependence, and ensures that it is of the SM. However, the A_1 mode frequency at low temperatures is unexpectedly low in comparison with the well-known value of 6.2 THz (Shapiro et al. 1967; Appendix 1).

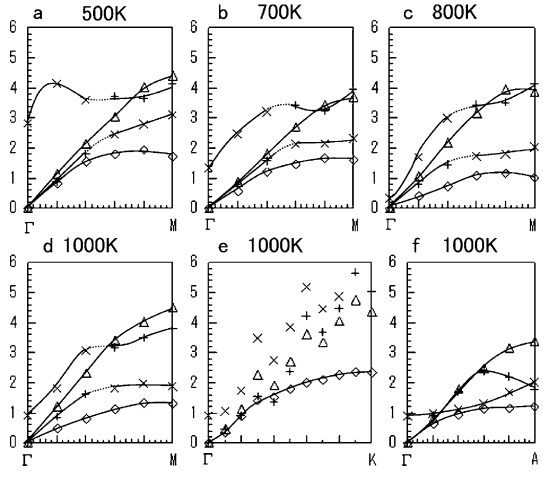

Fig. 6a–f Phonon dispersion relations of three acoustic and one optic soft branches constructed for atomic trajectories in a molecular dynamics simulation of quartz. **a** to **d** 500, 700, 800 and 1000 K in Γ-M direction. **e** and **f** Γ-K and Γ-A, respectively, at 1000 K. The four branches are named by atomic displacement patterns at $q = 0.1$. TA_1 Transversal acoustic branch with lowest-frequencies; TA_2 second-lowest branch; LA longitudinal acoustic branch; SM soft optic branch; Atomic displacement patterns for TA_1 and TA_2 at $q = 0.1$ are dominated by x and z components, respectively, for Γ-M (in **b***), by z and (x,-y), respectively, for Γ-K (in $\xi\xi 0$), and y (real part) + x (imaginary part) and y(re.) + xz(im.), respectively, for Γ-A. *Lines* only suggest probable dispersion relations. *Symbols* identify the continuities of eigenvectors: *two curves in* Γ-*M with dotted lines* between $q = 0.2$ and 0.3 could exchange the displacement patterns in that region as far as the continuities of atomic displacement patterns are concerned

Our polarization vectors for the lowest branch in this direction are dominated by TA components in the (001) plane, and only slightly modified by the SM character (Appendix 2): the displacement patterns almost comply with the antisymmetric Σ_2 rep (antisymmetric against the C_2^1 operation in this direction). Along Γ-M, the atomic displacement pattern, denoted as $TA_1(xy)$, gradually changes from that at point M (Fig. 7a) to the pure TA character at Γ by rotating and enlarging the vectors for Si1, O1, O3, O4 and O6.

On the other hand, the TA_2 and the SM branches in this direction of the MD crystal show unexpected behaviour at all the temperatures studied. The TA_2 modes are dominated by the displacements along [001], i.e. TA(z) (also in Σ_2), at small **q** up to about 0.2, but lose obvious continuity at $q = 0.3$. The TA(z) pattern is regained above $q = 0.4$ via TA(yz) at $q = 0.3$, but by the third-lowest mode (Fig. 6). The SM branch rises steeply from a low frequency at Γ with increasing **q**, but its atomic displacement pattern at $q = 0.3$ appears to be the

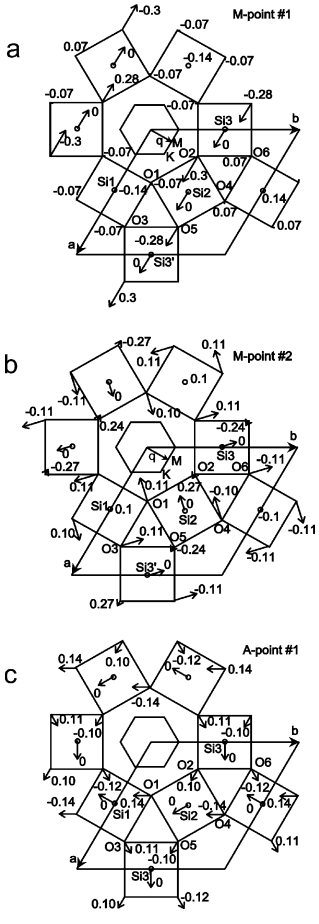

Fig. 7a–c Atomic displacement patterns in some points in the Brillouin zone, deduced from normal mode analyses for a β-quartz crystal in molecular dynamics simulation. The Brillouin zone is conveniently drawn by *small hexagons* inside the void spaces centring the origins of the unit cell. **a** The lowest M-point mode. Wave vector **q** is shown. **b** The second-lowest M-point mode. **c** The lowest A-point mode. **q** is perpendicular to the **a***–**b*** plane

same (in Σ_2) as that in TA_2: that is to say, the TA_2 and SM exchange their eigenvectors around **q** in 0.2 to 0.3.

The LA mode (in symmetric Σ_1 rep) takes the third-lowest position at the small **q** region with atomic displacements, TA(*y*), parallel with **q** (//**b***), but the branch wit h the TA(*z*) characters takes the third position in an intermediate region up to point M, as noted above (Fig. 6).

Γ-*K branches*

In this direction (Fig. 6e for 1000 K), the three acoustic branches are TA(*xy*), TA(*z*) and LA, which show less differences in frequencies at small **q**. The dispersion curves are not smooth except for the lowest branch. The four dispersion curves are considerably higher than those in Γ-M, and the polarization vectors in the lowest branch keep acoustic characters at small **q**, but not at **q** larger than 0.2, unlikely in Γ-M. These explain the negligibly small DS in this direction (Fig. 5e to h).

Γ-*A branches*

The lowest TA_1 branch in this direction lies low, almost equally in TA_1 in Γ-M. The contribution from this branch is also notably larger for the reflections in the FH (for example, 4 $\overline{3}$ 0 and 4 $\overline{2}$ 0 in Fig. 5i and j) than for other reflections, resulting in diffuse streaks extending into ± **c*** along the FH. The optic branch connected to the SM at Γ shows rather weak changes in frequency (Fig. 6f for 1000 K) and in displacement patterns with **q**.

Atomic displacement patterns

Group-theoretical analyses indicate that the polarization vectors in the M-point modes are real in both α- and *β*-quartz. Our MD values (obtained without symmetry constraint) were essentially real with negligibly small imaginary components. The polarization vectors in the lowest-frequency mode at point A in *β* quartz were also essentially real. Figure 7 shows the normalized eigenvectors to indicate such linear motions in the lowest modes at point M and A, and the second-lowest mode at point M, all in the *β* phase of the present MD crystal.

Discussion

In the quartz structure, we can see atomic chains running parallel with three directions of ⟨100⟩, as represented by −Si3(2/3)–O2(1/2)–Si2(1/3)–O5(1/2)–Si3′(2/3)- (Fig. 7), where, if the case of *β* quartz is taken, the *z* coordinates of the same types of atoms shown in parentheses are different by **c**/3 or 0 under the 6_2 (or 6_4) screw operations. This relation for the *z* coordinates is roughly maintained in the α phase at high temperatures.

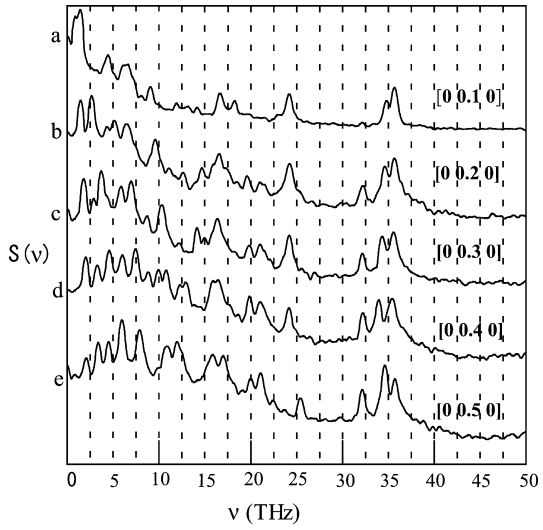

Fig. 8 Power spectra $S(\nu)$ at different wave vectors on Γ-M calculated on atomic trajectories in an NVE ensemble molecular dynamics simulation at 300 K. *System size* 9000 atoms; *record size* 4096 of 40 960 steps. $S(\nu)$ in a logarithmic scale

In this arrangement, not all but some hk0 reflections in the FH and hk3 reflections in the second hexagon can have strong intensities. If the sum of the inner products of scattering vector $\mathbf{Q} = 2\pi(\mathbf{H}_{hk\ell\}} + \mathbf{q})$ for these $\mathbf{H}_{hk\ell}$ and atomic polarization vector **e** over the unit cell is significant, and the relevant frequency is low enough, we may have some amount of DS around the relevant $\mathbf{H}_{hk\ell}$ in the directions of the wave vectors **q**.

We explain here the specific atomic displacements in the lowest branch in Γ-M, effective enough to produce the DS in the FH of the $\xi\eta 0$ plane. The lowest-frequency mode at point M is characterized by the antiparallel motions, in nearly equal amplitudes, of atoms in −Si3–O2–Si2–O5–Si3′ chains in [100] (Fig. 7a for **q** parallel with **b***). If **q** approaches from M to Γ, the displacements of the atoms linking the two parallel chains are increasingly enlarged and oriented toward [100], resulting in all the displacements being approximately parallel and equal in amplitude to each other. In this state, the right-hand term of Eq. (3) is approximated by

$$\mathbf{Q}\cdot\mathbf{e}(j\mathbf{q})\sum_k m_k^{-1/2} f_k(\mathbf{Q})\exp[-W_k(\mathbf{Q})]\exp[2\pi i\mathbf{H}\cdot\mathbf{r}(k)]\ ,$$

where polarization vector $\mathbf{e}(k|j\mathbf{q})$ is replaced by $\mathbf{e}(j\mathbf{q})$, common to all the atoms involved. Vectors **Q**, which are associated by large DS, must necessarily be oriented parallel or nearly parallel with $\mathbf{e}(\mathbf{q})$. Reflection 4 $\overline{2}$ 0 in the FH, having a predominant static structure factor for the quartz structure, satisfies this condition almost perfectly with $q = 0$, or nearly so with non-zero **q** parallel with **b***. Other reflections such as 4 $\overline{1}$ 0, 4 $\overline{3}$ 0 and 400 in the FH, which lie with angle ϕ within 30° from the line passing Γ and perpendicular to that **q**, also have large structure factors, and provide significant dynamical structure factors depending on cos ϕ. The six directions

of **q** give rise to the six diffuse lines which merge to form the FH.

The DS streaks observed in the higher reciprocal lattice planes of the MD crystal are parallel with the FH in the $\xi\eta 0$ plane, ensuring that the Γ-M branches are also responsible for these. For reflection 203 belonging to the second hexagon in the $\xi\eta 3$ plane (Fig. 2b) and also to the largest structure factor group, the lowest and third-lowest branches make a major contribution to the DS (Fig. 5d). The atomic displacements in these branches are not parallel with the scattering vectors **Q** in the higher reciprocal lattice planes, but have some degree of parallel components with **Q**, resulting in the DS of the second hexagon in the $\xi\eta 3$ plane. With respect to the third-lowest branch, we recall that the atomic displacement patterns in this branch in Γ-M largely change from LA at small **q** to TA(z) at M via TA(yz) in an intermediate region.

The atomic displacement patterns in the TA_1 branch in Γ-A are dominated by TA(xy) components, also rich in parallel components in $\langle 100\rangle$ and $\langle 200\rangle$, with the same sign for the majority of atoms. In Fig. 7c, the polarization vectors at zone boundary A in TA_1, symmetrically real, are illustrated, from which the displacement patterns gradually change to more pronounced TA ones with decreasing **q** along Γ-A. These modes contribute to the DS extending into $\pm$**c*** around each Bragg spot and especially around the FH of the $\xi\eta 0$ plane and the second hexagon of the $\xi\eta 3$ plane.

The origin of the DS in the FH has been considered to be dynamic (Tendeloo et al. 1976), mainly contributed by the lowest-frequency phonon branches in Γ-M (Bauer et al. 1971). The present MD study of the DS in the FH is in harmony with these previous studies for the origin of the DS, but showed diffuse tails radiating parallel with **a*** and its equivalent directions from Bragg reflections. We consider that the diffuse tails are comparable with the INC satellite reflections with respect to their origin being related to the lowest-frequency phonon modes in Γ-M. The size of our MD crystal is too small to give rise to satellite spots as observed in real quartz crystals, which arise from the condensation of phonons at $q \ll 0.1$ (for example, Dolino et al. 1984; Berge et al. 1986).

Concluding remarks

The present molecular dynamics study of the quartz structure shows that the lowest-frequency branches are highly anisotropic in frequencies in the plane perpendicular to **c***, lower in Γ-M and higher in Γ-K. The lowest branch (second-or third-lowest branch for some reflections) in Γ-M is temperature-dependent and causes radial DS around Bragg spots and non-radial DS in hexagonal prismatic surfaces at high temperatures. The TA(xy) displacements of atoms in Γ-M and Γ-A are especially effective in enhancing the DS in the FH extended in $\pm$ **c*** in relation with the quartz structure. When the MD crystal was large enough, we could observe incommensurate satellite reflections.

The present MD results indicate that the characteristic DS in quartz is purely a phenomenon arising from phonon behaviour, together with the fact that the DS in the fourth hexagon takes place at low temperatures in the α phase, where no dynamical structure disturbance other than phonons is effective. The phonon dispersion relations for the three acoustic branches in the present MD crystal are apparently quite comparable with those in previous neutron inelastic experiments as far as the frequencies are concerned. However, the detailed analysis of atomic displacement patterns showed some points which may need further investigation, mainly concerning the behaviour of acoustic TA(z) and optic SM branches in Γ-M.

Acknowledgements The computer program for molecular dynamics simulations, CTPMD, was provided by Professor M. Matsui of Himeji Institute of Technology, to whom the authors express sincere thanks. This study was supported by the grant-in-aid for Scientific Research of JSPS (no. 14540446).

References

Arnold H (1965) Diffuse Röntgenbeugung und Kooperation bei der α-β-Umwandlung von Quartz. Z Kristallogr 121: 145–157

Barron THK, Huang CC, Pasternak A (1976) Interatomic forces an lattice dynamics of α-quartz. J Phys Solid State Phys 9: 3925–3940

Bauer KH, Jagodzinski WH, Dorner B, Grimm H (1971) The inelastic nature of diffuse X-ray scattering near the α–β transition in quartz. Phys State Solids (B) 48: 437–443

Berge B, Bachheimer JP, Dolino G, Vallade M, Zeyen CME (1986) Inelastic neutron scattering study of quartz near the incommensurate phase transition. Ferroelectrics 66: 73–84

Boysen H, Dorner B, Frey F, Grimm H (1980) Dynamic structure determination for two interacting modes at the M point in α- and β-quartz by inelastic neutron scattering. J Phys (C) Solid State Phys 13: 6127–6146

Dolino G, Bachheimer JP, Berge B, Zeyen CME (1984) Incommensurate phase of quartz: I. Elastic neutron scattering. J Phys France 45: 361–371

Dolino G, Berge B, Vallade M, Moussa F (1992) Origin of the incommensurate phase of quartz: I: Inelastic neutron scattering study of the high temperature β phase of quartz. J Phys I France 2: 1461–1480

Dove M (1987) Molecular dynamics simulations in the solid state sciences. In: Salje EKH (ed) Physical properties and thermodynamic behaviour of minerals. NATO ASI Series C: mathematical and physical sciences, vol. 225, Reidel, Dordrecht, pp 501–590

Dove M (1993) Introduction to lattice dynamics. Cambridge University Press, Cambridge

Gouhara K, Li YH, Kato N (1983) Observation of satellite reflections in the intermediate phase of quartz. J Phys Soc Jpn 52: 3697–3699

Kihara K (1990) An X-ray study of the temperature dependence of the quartz structure. Eur J Mineral 2: 63–77

Kihara K (2001) Molecular dynamics interpretation of structural changes in quartz. Phys Chem Miner 28: 365–376

Kihara K, Matsui M (1999) Molecular dynamics study of structural changes in berlinite. Phys Chem Miner 26: 601—614

Miyake A, Hasegawa H, Kawamura K, Kitamura M (1998) Symmetry and its change in reciprocal space of a crystal simulated by molecular dynamics: application to quartz. Acta Crystallogr (A) 54: 330–337

Müser MH, Binder K (2001) Molecular dynamics study of the α–β transition in quartz: elastic properties, finite size effects, and hysteresis in the local structure. Phys Chem Miner 28: 746–755
Ohsumi K, Miyata Y, Hagiya K, Ohmasa M (2002) Crystallographic study on the incommensurate phase of quartz by SR. Acta Crystallogr (A) 58 (Supplement): C369
Shapiro SM, O'Shea DC, Cummins HZ (1967) Raman scattering of the alpha–beta phase transition in quartz. Phys Rev Lett 19: 361–364
Tendeloo J, Landuyt J, Amelinckx S (1976) The $\alpha \rightarrow \beta$ phase transition in quartz and $AlPO_4$ as studied by electron microscopy and diffraction. Phys State solids (A) 33: 723–735
Tsuneyuki S, Aoki H, Tsukada M, Matsui Y (1990) Molecular-dynamics study of the α to β structural transition of quartz. Phys Rev Lett 64: 776–779
Vallade M, Berge B, Dolino G (1992) Origin of the incommensurate phase of quartz: II. Interpretation of inelastic neutron scattering data. J Phys I France 2: 1481–1495
Willis BTM, Pryor AW (1975) Thermal vibrations in crystallography. Cambridge University Press, Cambridge
Worlton TG, Warren JL (1972) Group-theoretical analysis of lattice vibrations. Comp Phys Comm 3: 88–117
Zarka A, Capelle B, Petit M, Dolino G, Bastie P, Berge B (1988) Evidence of a single q incommensurate phase in quartz by synchrotron X-ray diffraction. J Appl Crystallogr 21: 72–73

Appendix 1

In our analysis, the frequencies of fluctuations are calculated for all the modes at given wave vectors. Problems occur for the acoustic modes at Γ: the amplitudes calculated from Eq. (7) for these modes at Γ are finite, depending on the size of crystal. Our frequencies of the acoustic modes at the Γ-point are not of significance for real crystals: instead, the expected value of zero frequency is assigned in Fig. 6.

The low-frequency branches including the SM branch appear quite comparable with those of the neutron inelastic measurements (Dolino et al. 1992) as far as the β phase and high temperatures in the α phase are concerned. The success in extracting the remarkable temperature dependence of the SM frequencies from the MD crystal shows a preferable aspect of this normal mode analysis in comparison with lattice dynamical calculations (in a harmonic approximation). The low-frequency SM at low temperatures reminds us of the existence of a low-frequency satellite spectrum at 4.4 THz at room temperature in a Raman measurement (Shapiro et al. 1967), which becomes the true SM with increasing temperature. However, our SM branch at low temperatures is apparently too low in comparison with that of lattice dynamical calculations (for example, Barron et al. 1976). This inconvenience remains unanswered in this study.

We have two broad bands of optic modes at about 4 and 6.5 THz in the low-frequency region in the power spectra for $q = 0.1$ on Γ-M, calculated as in Kihara and Matsui (1999) for the atomic trajectories, which are quite successful in extracting spectral features characteristic of the quartz structure (Fig. 8). Our low-frequency optic modes at Γ in the normal mode analysis at 300 K are of the A_1 at 3.4 THz and of an E rep at 4.1 THz, which could be assigned to the band at 4 THz.

Appendix 2

As shown in the text, the lowest branch in Γ-M is predominantly of transversal acoustic with major atomic displacements only in the x direction at small **q** parallel with **b***. We assumed that the displacements of an atom in the y and z directions were given only by the optic SM, i.e.

$$\delta_{AO}\, p(AO)_\alpha = \delta_O\, p(O)_\alpha\, \lambda_O \quad , \tag{6}$$

where $p(AO)_\alpha$ is of either the y or z component of the normalized atomic polarization vector in the AO mixed mode, i.e. $TA_1(xy)$, and $p(O)_\alpha$ is that in the unmixed optic SM. The coefficients δ_{AO} and δ_O are the amplitudes of the AO mixed and unmixed optic soft modes, respectively. The polarization vectors $p(AO)_y$ and $p(AO)_z$ both separately provide the estimation of λ_O, the result measured in the ratio to that for SM at $q = 0$. If the corresponding values for $p(O)_y$, $p(O)_z$ and δ_O ($= 5.05$ Å) at $q = 0$, and δ_{AO} ($= 9.38$ Å) at $q = 0.1$, all at 1000 K, are taken, Eq. (6) provides about 0.74(9) and 0.78(9), respectively, as the averages over six atoms to λ_O. Three atoms were not used because their polarization vector components $p(O)_y$ (for Si1, O2 and O5) and $p(O)_z$ (for Si1, Si2 and Si3) were essentially zero (Fig. 7). These values suggest that the atomic displacements in TA_1 at $q = 0.1$ in Γ-M may involve optic SM components amounting to about 75% of those values at Γ, much smaller than the contribution from TA components with larger amplitude and polarization vectors.